Journal of the European Ceramic Society 41 (2021) 4835–4840

Contents lists available at ScienceDirect

Journal of the European Ceramic Society

journal homepage: www.elsevier.com/locate/jeurceramsoc

High quality factor cold sintered LiF ceramics for microstrip patch antenna applications

Bing Liu [a,b,*], Ke Sha [a], Ying Qiang Jia [b], Yu Hui Huang [b], Cheng Chao Hu [c], Lei Li [b,**], Da Wei Wang [d], Di Zhou [e], Kai Xin Song [a,**]

[a] College of Electronic Information and Engineering, Hangzhou Dianzi University, Hangzhou, China
[b] School of Materials Science and Engineering, Zhejiang University, Hangzhou, China
[c] College of Materials Science and Engineering, Liaocheng University, Liaocheng, China
[d] Shenzhen Institutes of Advanced Technology, Chinese Academy of Sciences, Shenzhen, China
[e] School of Electronic Science and Engineering, Xi'an Jiaotong University, Shaanxi, China

ARTICLE INFO

Keywords:
Fluoride
Cold sintering
Microwave dielectric properties
Microstrip patch antenna

ABSTRACT

Cold sintering is adopted to pre-densify LiF ceramics, where the relative density increases significantly from 72.1 % at 125 MPa to 88.9 % at 500 MPa. The following post-annealings at 800 °C lead to further optimizations of densification, and near-full densifications with relative densities of 95.6 % and 97.6 % are achieved at 375 and 500 MPa, respectively. *Qf* value increased with increasing uniaxial pressure until it reaches the maximum value of 134,050 GHz at 375 MPa, which is 1.82 times higher than that via conventional sintering (73,800 GHz). ε_r and τ_f are mainly determined by the relative density, and the optimum microwave dielectric properties are obtained as follows: $\varepsilon_r = 8.45$, $Qf = 134{,}050$ GHz, $\tau_f = -135$ ppm/°C. A microstrip patch antenna is designed and fabricated using the LiF ceramic as the substrate, which gives an S11 of –20.3 dB, a simulated high efficiency of 90.5 %, and a gain of 4.25 dB at the resonant frequency of 6.81 GHz.

1. Introduction

With the merits of low profile, lightweight, easy fabrication, and low cost, microstrip patch antennas (MPA) are popular RF components that have been widely used in handheld communication devices such as mobile phones and tablets [1]. The efficient implementation of MPA requires high-performance microwave dielectric ceramics since the dielectric substrate plays a vital role in optimizing the antenna performances, such as radiation coefficient and efficiency [2,3]. Nowadays, with the operating frequencies of mobile communications moving towards higher-frequency bands such as sub-6 GHz and millimeter-wave range, dielectric ceramics with low dielectric constant ($\varepsilon_r < 15$) have received extensive attention since the signal delay time is proportional to $f\sqrt{\varepsilon_r}$ [4–6]. On the other hand, a high quality factor (*Qf*) is urgently required as the signal attenuation is highly sensitive to the dielectric loss [7]. The temperature coefficient of resonant frequency (τ_f) is another key parameter but less critical in applications where the electromagnetic wave propagates, such as microwave substrates [8,9].

Dielectric materials for microwave applications have been researched for decades. Among them, researches on the low-ε_r and high *Qf* materials are mainly focused on the oxides, including silicates [10–13], germanates [14,15], borates [8,9,16], aluminates [17–19], phosphates [20,21], etc. Recently, researchers started to expand the search of low-ε_r candidates to fluorides and fluorine-containing ceramics [22–24]. In 2004, Geyer et al. reported the dielectric properties of LiF single crystal, where excellent microwave dielectric properties with a low ε_r of 9.0 and ultra-high *Qf* value of 192,400 GHz were obtained [25]. Inspired by this, in 2019, Song et al. have systematically prepared LiF ceramics via a conventional solid-state reaction method, while the optimum *Qf* value obtained was only 73,880 GHz [22]. According to Song et al., the large disparity in *Qf* value is mainly ascribed to the low relative density (90.2 %) of LiF ceramics, and it is difficult to further improve the densification via conventional sintering owing to the inferior surface free energy of LiF (~340 erg/cm^2) [22].

Cold sintering (CS) is a novel sintering technique based on the dissolution-precipitation densification mechanism [26]. During CS, with the aid of transient solvent and uniaxial pressure, the mass transport/diffusion between particles can be significantly accelerated, thus

* Corresponding author at: College of Electronic Information and Engineering, Hangzhou Dianzi University, Hangzhou, China.
** Corresponding authors.
E-mail addresses: liubing@hdu.edu.cn (B. Liu), zjulilei@zju.edu.cn (L. Li), kxsong@hdu.edu.cn (K.X. Song).

https://doi.org/10.1016/j.jeurceramsoc.2021.03.052
Received 1 January 2021; Received in revised form 22 March 2021; Accepted 24 March 2021
Available online 29 March 2021

promoting densification [27–29]. Besides, subsequent post-annealings of cold sintered ceramics have been widely confirmed efficient in further improvement of densification [30,31]. Hence, given the great potential of *Qf* improvement in LiF ceramics, in this work, cold sintering processes with various uniaxial pressures (125–500 MPa) are adopted to pre-densify the LiF ceramics and then followed by subsequent post-annealing treatments at 800 °C for 3 h. The evolutions of densification and microstructure are systematically investigated together with their effects on the microwave dielectric properties. Furthermore, an MPA prototype is designed and fabricated using LiF ceramic as the dielectric substrate. An extensive analysis of the radiation coefficient, VSWR (Voltage Standing Wave Ratio), radiation patterns, gain, and efficiency of the fabricated antenna is presented.

2. Experimental procedure

The high-purity raw powder of LiF (99.99 %) was purchased from Aladdin Chemical Reagent Co., Ltd. Before weighing, the raw powder was dried at 150 °C for 6 h to remove potential moisture and then mixed with 10 wt% of deionized water. The mixtures were then placed into a cylindrical die and pressed into pellets with 12.7 mm in diameter and 5 mm in height under uniaxial pressures of 125, 250, 375, and 500 MPa, respectively. The dwelling temperature/time during the cold sintering process was set as 150 °C/1 h. After cold sintering, the samples were post-annealed at 800 °C for 3 h to achieve further densification. A square-shaped die with a dimension of 30 mm was adopted to fabricate the LiF antenna substrate. After cold sintering (375 MPa) and post-annealing treatments, the substrate was pasted with Cu electrodes and then assembled with an SMA (Subminiature version A) connector. The simulation of antenna performance was carried out using CST microwave studio 2020 software.

The relative densities of LiF ceramics were evaluated based on their mass and dimensions. The phase compositions were identified using the X-ray diffractions (XRD: D/MAX 2550/PC, Rigaku). The microstructural evolution of the as-cold sintered samples was observed from the fractured surfaces using scanning electron microscopy (SEM: SIGMA 300, ZEISS). While, the microstructures of the post-annealed ceramics were revealed from the polished and thermally etched surfaces. The thermal etching process was carried out at 750 °C for 30 min. The grain sizes and distributions were obtained from the SEM images using ImageJ software [32]. ε_r and τ_f values were measured by the paralleling plate method using a vector network analyzer (E5061B, Keysight). τ_f value was calculated based on the resonant frequency shift from 20 °C to 80 °C. *Qf* values were evaluated at around 10 GHz using a silver-coated cavity connected to the network analyzer.

3. Results and discussion

The XRD patterns of LiF raw powder and cold-sintered ceramics under various uniaxial pressures are shown in Fig. 1(a). All the diffraction patterns can be well indexed according to the standard PDF card of LiF (JCPDS card #45-1460). No apparent changes in peak position and intensity are noticed among samples, indicating that the CS process and applied uniaxial pressure would not affect the resulting phase compositions. Fig. 1(b) gives the relative density of cold-sintered LiF ceramics as a function of uniaxial pressure. The relative density obtained under the pressure of 125 MPa is 72.1 %, higher than the regular dry-pressed ceramic compacts (50 %–70 %) [27]. This indicates that the low solubility of around 0.29 g/100 ml for LiF is high enough to activate the dissolution-precipitation process and thus promotes the densification [33]. The relative density increases rapidly with increasing pressure until it saturates at around 88.9 % at 500 MPa, indicating that the uniaxial pressure plays a vital role in the densification process. The relative density of 88.9 % is much higher than the ideal packing density of rigid spherical particles (74 %). This could be attributed to the cubic-shaped particles of LiF raw powders shown in the supporting

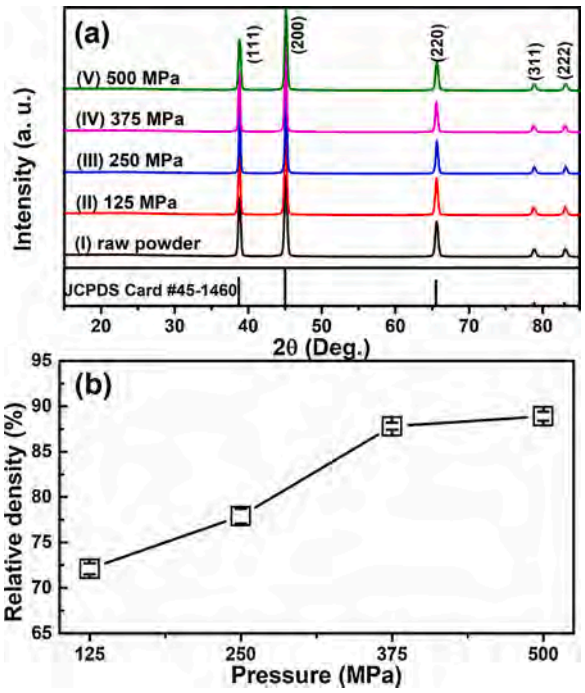

Fig. 1. XRD patterns of (a) LiF raw powder and cold sintered ceramics under various pressures. (b) The variation of the relative density of as-cold pressed LiF ceramics with uniaxial pressure.

information (Fig. S1), which allows higher packing density than the spherical particles. Moreover, during the dissolution-precipitation process, the shapes of LiF particles could be modified to achieve a further densification. On the other hand, according to the previous works on cold sintered NaCl and H_3BO_3 ceramics, materials with low hardness could be reshaped and rearranged under a certain amount of external mechanical pressure, which is beneficial to the densification process [9, 28]. Since LiF has a low Mohs hardness of around 3 [34], the improvement of relative density at high pressure could also be ascribed to microstructure optimization.

Fig. 2 gives the SEM images of the fractured surfaces of cold pressed LiF ceramics under various uniaxial pressures. As shown in Fig. 2(a), the grain size and morphology of raw powder are preserved at a low pressure of 125 MPa. The microstructure gets denser with increasing uniaxial pressure, which is in accord with the improvement of relative density shown in Fig. 1(b). On the other hand, the grain sizes in Fig. 2(c, d) are surprisingly much smaller than those of Fig. 2(a, b). Considering the low Mohs hardness of 3 in LiF, it is reasonable to infer that the large particles are prone to be compressed and fractured into small ones when applying a high uniaxial pressure of above 250 MPa. Similar results were also reported in gypsum ceramics under a pressure of 400 MPa and $CaCO_3$ ceramic under 500 MPa [27,35].

The post-annealing process is applied to achieve the further densification of LiF ceramics. SEM images of the post annealed LiF ceramics under various uniaxial pressures are presented in Fig. 3. A porous microstructure with faint grain boundaries is obtained in the post-annealed LiF ceramics with the uniaxial pressure of 125 MPa. With increasing pressure, the pores decrease significantly at 250 MPa and almost vanish at higher pressures. The porous microstructure optimization is in good accordance with the improvement of relative density shown in Fig. 4(a), where the relative density increases from 78.9 % at 125 MPa to 97.6 % at 500 MPa.

Meanwhile, with increasing uniaxial pressure, the grain boundary tends to get clearer. The average grain size increases monotonously until it reaches the maximum value of 101 μm at 375 MPa and decreases slightly to 95 μm at 500 MPa. The significant improvement of grain size

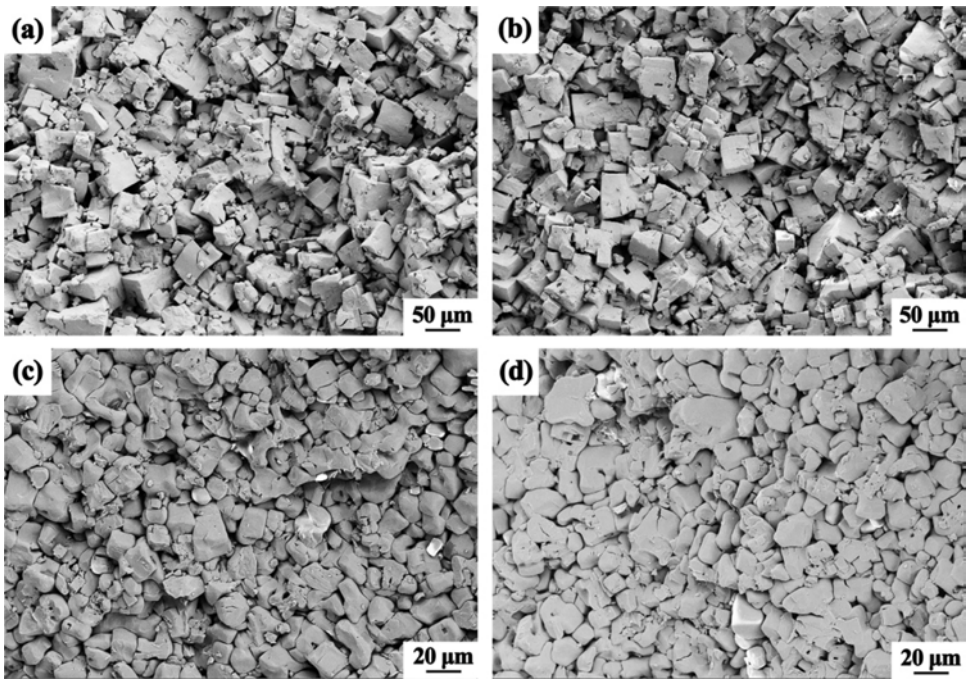

Fig. 2. SEM images of the fractured surfaces of the cold pressed LiF ceramics under various uniaxial pressure (a) 125 MPa, (b) 250 MPa, (c) 375 MPa and (d) 500 MPa.

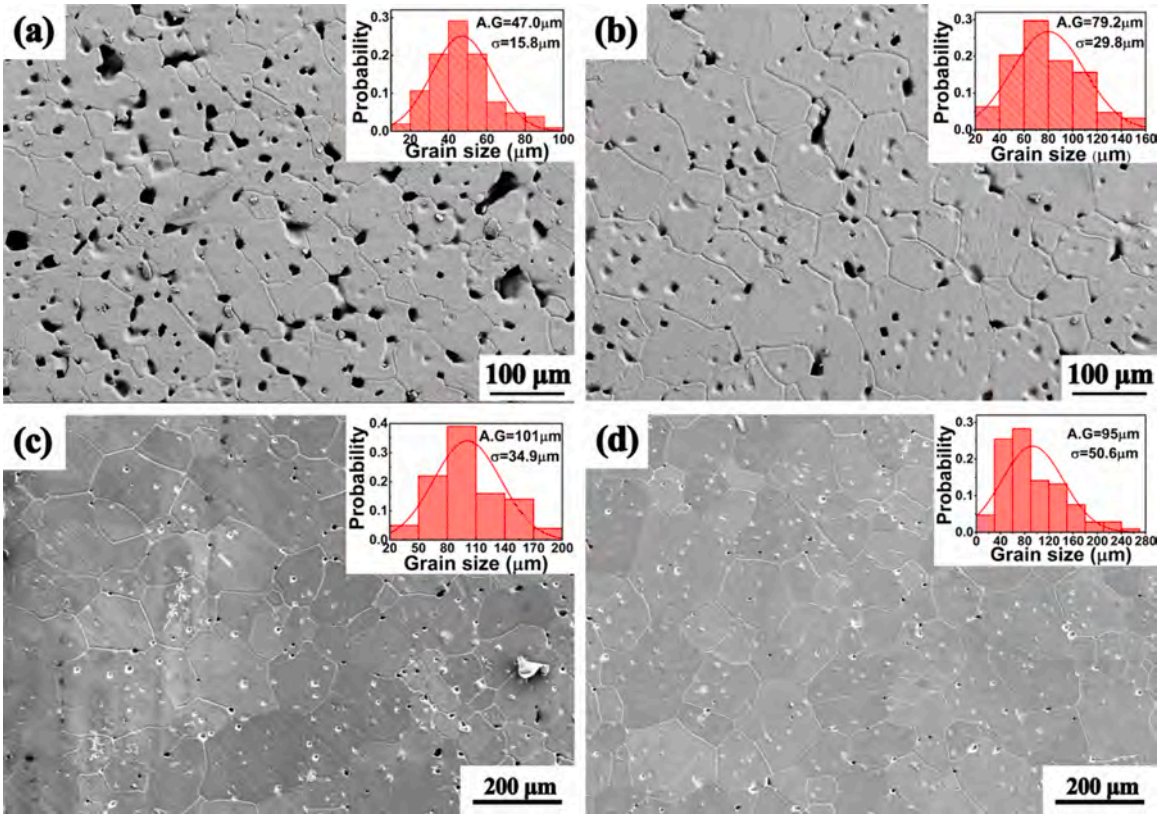

Fig. 3. SEM images of post annealed LiF ceramics under various uniaxial pressures (a) 125 MPa, (b) 250 MPa, (c) 375 MPa and (d) 500 MPa. The inset figures give the average grain size (AG), grain size distribution, and standard deviation (σ) of each composition.

is attributed to the higher packing density after cold sintering, leading to rapid mass transport and eliminating the pores between grains. Meanwhile, the average grain size after post-annealing is overall larger than the corresponding as-cold sintered sample, indicating that post-annealing treatment is beneficial to both the grain size and densification. The fractured small grain size obtained in Fig. 2(c) and (d) does not affect the large grain size after post-annealing. Moreover, it is worthy to note that the uniaxial pressure of 375 MPa is a significant threshold for

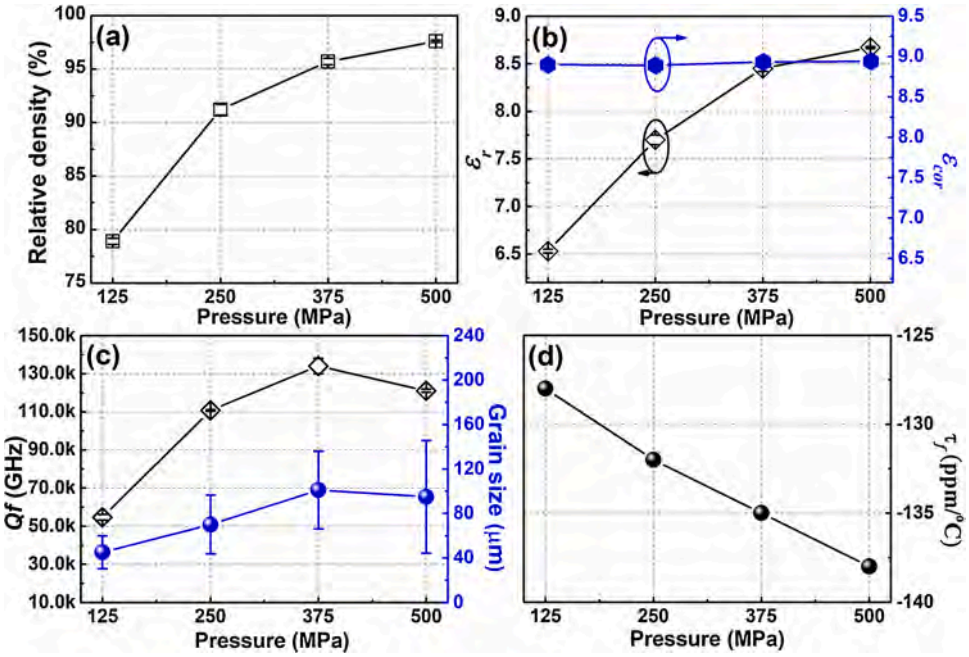

Fig. 4. (a) Relative density, (b) ε_r, ε_{cor} values, (c) *Qf* values and average grain size, and (d) τ_f value of LiF ceramics as functions of uniaxial pressures.

the densification and microstructure evolution, which might impact the microwave dielectric properties.

As shown in Fig. 4(b), ε_r of the post annealed LiF ceramics ascends with increasing uniaxial pressure, from 6.5 at 125 MPa to 8.7 at 500 MPa. Meanwhile, the changing trend of ε_r is quite similar to the relative density, indicating that eliminating pores with increasing uniaxial pressure should play the determining role in controlling ε_r. Moreover, based on the previous results of Alford et al., the influence of porosity (*P*) can be corrected using the following equation [36].

$$\varepsilon_r = \varepsilon_{cor}\left(1 - \frac{3P(\varepsilon_{cor}-1)}{2\varepsilon_{cor}+1}\right) \quad (1)$$

where, ε_{cor} denotes the porosity corrected dielectric constant, and the calculated values in this work are plotted in Fig. 4(b). No apparent variation of ε_{cor} is observed, and all the values remain at around 8.9, which further confirms that the porosity mainly controls ε_r.

Qf value is determined from both the intrinsic and extrinsic parameters. In this work, with the absence of structural transitions and impurity phases, the variation of *Qf* value should be mainly discussed from extrinsic factors such as relative density and microstructural homogeneity. Fig. 4(c) gives the *Qf* values and average grain sizes as functions of uniaxial pressure. With increasing the pressure from 125 MPa to 375 MPa, *Qf* value increases rapidly from 54,600 GHz to 134,050 GHz, which corresponds to the improvement of densification and grain size. The ultra-high *Qf* value of 134,050 GHz is 1.82 times higher than the reported values (73,880 GHz) via conventional sintering, indicating the significant advantages of cold sintering in optimizing the microstructure and subsequently the microwave dielectric properties. On the other hand, further increasing the pressure will lead to a slight decrease of *Qf* value to 121,080 GHz, despite that the relative density at 500 MPa (97.6 %) is slightly higher than that of 375 MPa (95.7 %). The drop of *Qf* value at 500 MPa could be ascribed to its smaller average grain size and larger standard deviation (50.6 μm) of grain size distribution, which indicates a less homogeneous microstructure. Actually, for cold-sintered ceramics with nearly full densification, plenty of works have shown that the microstructure homogeneity plays a critical role in determining the resultant dielectric or mechanical properties [27,28,37].

τ_f value indicates a downward trend with increasing uniaxial pressure, from –128 ppm/°C to –138 ppm/°C at 125 MPa and 500 MPa, respectively. Table 1 lists the relative density and microwave dielectric properties of the present ceramics and the optimum microwave dielectric properties (ε_r = 8.45, *Qf* = 134,050 GHz, τ_f =–135 ppm/°C) are obtained under the uniaxial pressure 375 MPa. Table 2 lists the sintering temperatures and microwave dielectric properties of a series of low-ε_r dielectric ceramics. By comparison, LiF ceramics obtained in this work exhibit a good combination of microwave dielectric properties and have a relatively low sintering temperature.

The microstrip patch antenna consists of three parts, i.e., the top radiating patch, the middle dielectric substrate, and the bottom electrode as the ground plane [38]. Fig. 5(a) gives the schematic picture of the configuration and geometry for the designed antenna. The dimension of the LiF substrate is 30 × 30 × 1.1 mm, and the ground plane has the same length/width as the substrate. The length and width of the patch are designed as 11.9 and 8.5 mm, the width of the microstrip line is 1.2 mm. S11 is the most commonly quoted parameter in the design of antennas. According to Eq. (2), S11 represents the ratio of input power (P_1) to reflected power (P_2) and is also known as the return loss. If S11 = 0 dB, then all the power is reflected from the antenna, and noting is radiated. If S11 = –10 dB, then 90 % of the power is transmitted with 10 % reflected. Therefore, for practical applications, the –10 dB value is adopted as the base value and regarded as acceptable for wireless

Table 1
Summary of relative density and microwave dielectric properties of LiF ceramics prepared at various uniaxial pressures.

uniaxial pressure	ρ (%) (cold pressed)	ρ (%) (post annealed)	ε_r	ε_{cor}	*Qf* (GHz)	τ_f (ppm/°C)
125 MPa	72.1 ± 0.6	78.9 ± 0.3	6.53 ± 0.02	8.90	54,600 ± 1520	–128
250 MPa	77.9 ± 0.8	91.2 ± 0.5	7.70 ± 0.05	8.89	110,800 ± 450	–132
375 MPa	87.8 ± 0.4	95.6 ± 0.3	8.45 ± 0.03	8.93	134,050 ± 4030	–135
500 MPa	88.9 ± 0.5	97.6 ± 0.1	8.67 ± 0.01	8.94	121,080 ± 860	–138

Table 2
Comparing sintering temperature, crystal structure, and microwave dielectric properties of some typical materials with low ε_r.

Material	ST (°C)	ε_r	Qf (GHz)	τ_f (ppm/°C)	Reference
$Mg_2Al_4Si_5O_{18}$	1450	6.2	40,000	–25	[10]
Zn_2SiO_4	1325	6.6	198,400	–41.6	[11]
Mg_2SiO_4	1450	7.5	112,780	–63	[12]
$MgSiO_3$	1380	6.7	121,200	–17	[13]
Zn_2GeO_4	1300	6.9	102,700	–32	[14]
Mg_2GeO_4	1200	6.5	91,000	–28	[15]
$Mg_3B_2O_6$	1300	7.0	230,900	–58	[16]
$Li_6B_4O_9$	640	5.95	41800	–72	[8]
H_3BO_3	Room temperature /P = 100 MPa	2.84	146,000	–242	[9]
$MgAl_2O_4$	1650	8.5	105,000	–63	[17]
$ZnAl_2O_4$	1375	8.5	56,000	–79	[18]
$CaAl_2O_4$	1450	8.9	91,350	–55	[19]
$LiMgPO_4$	950	6.6	79,100	–60	[20]
$SrCuP_2O_7$	925	7	101,110	–62	[21]
$NaCa_4V_5O_{17}$	840	9.72	51,000	–84	[42]
$Mg_2Co(VO_4)_2$	1000	9.2	107,500	–97	[43]
$Ba_3Mg(V_2O_7)_2$	660	10.3	43,400	–46.87	[44]
LiF	800	8.45	134,050	–135	**This work**

communications. Fig. 5(b) plots the simulated and measured S11 parameter of the antenna. The simulated antenna resonates at 6.80 GHz with a good S11 of –18.3 dB, covering a –10 dB bandwidth of 102 MHz. The measured S11 curve is in good agreement with the simulated one, with a resonant frequency of 6.81 GHz, a better return loss of –20.3 dB, and a relatively larger bandwidth of 148 MHz. The excellent S11 value indicates that nearly all the input power could be radiated through the antenna.

$$S11(\mathrm{dB}) = -10 \times \lg(P_1/P_2) \quad (2)$$

Fig. 5(c) plots the measured VSWR curve of the present antenna. VSWR is another factor representing the power reflection of antennas. The antenna's ideal VSWR value is 1 dB, meaning that all the input energy is transmitted. Typically, the VSWR value should be no more than 2.5 dB, and the smaller the value, the better the performance [39]. For the present antenna, the measured VSWR curve presents an excellent value of 1.21 at the resonant frequency of 6.81 GHz, which further confirms the good results of its reflection coefficient. Fig. 5(d) shows the simulated antenna radiation gain and efficiency as functions of frequency. In the frequency range of 6.6–7 GHz, the gain varies slightly in the range of 4.25–4.5 dB, and the efficiency could remain higher than 90.5 %. The simulated radiation patterns of the E-plane and H-Plane are shown in Fig. 5(e) and (f), respectively. For both planes, the copolar fields are much stronger than that of the crosspolar fields in the boresight direction ($\theta = 0°$) [40,41]. In summary, the excellent antenna performances and microwave dielectric properties of LiF ceramics, together with the low processing temperature, indicate great potentials for wireless communication applications.

4. Conclusions

The effects of cold sintering on the densification and microwave dielectric properties of LiF ceramics are systematically investigated in this work. The relative density of as-cold sintered LiF ceramics increases from 72.1 % to 88.9 % with increasing the uniaxial pressure from 125 MPa to 500 MPa. Subsequent post-annealing treatment leads to significant grain growth and further optimization of densification, where near-full densifications with relative densities of 95.6 % and 97.8 % are achieved at 375 and 500 MPa, respectively. The optimization of microstructure leads to a significant improvement of microwave dielectric properties. The maximum Qf value of 134,050 GHz is obtained under the uniaxial pressure of 375 MPa, which is 1.82 times higher than that via conventional sintering (73,880 GHz). The optimum microwave dielectric properties are obtained as follows: $\varepsilon_r = 8.45$, $Qf = 134{,}050$ GHz, $\tau_f = -135$ ppm/°C. A microstrip patch antenna is designed and fabricated using LiF ceramics as the substrate. The antenna resonates at the frequency of 6.81 GHz, exhibits an S11 of –20.3 dB and a –10 dB

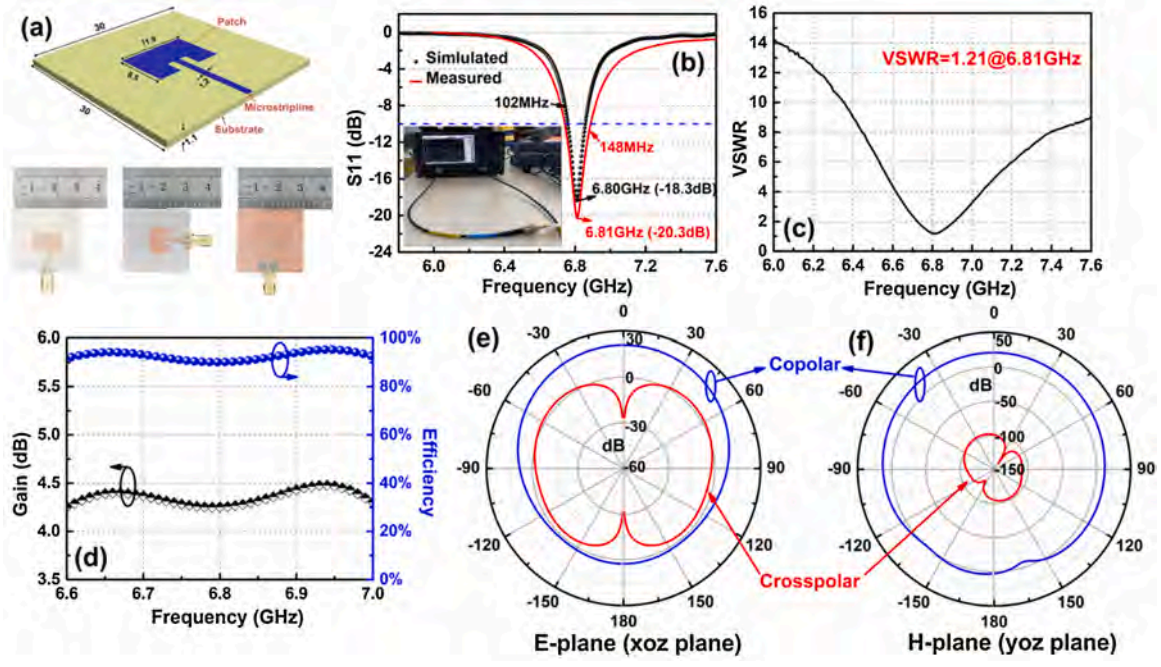

Fig. 5. (a) Schematic figure of the configuration and geometry for the designed patch antenna (unit: mm) and the photos of the front and rear view of the fabricated antenna. (b) The simulated (black circles) and measured (red curve) S11 curves and (c) the measured VSWR of the fabricated patch antenna. (d) The simulated antenna radiation gains and efficiencies verse frequency. The simulated radiation patterns of (e) E-plane and (f) H-plane (For interpretation of the references to colour in this figure legend, the reader is referred to the web version of this article).

bandwidth of 148 MHz. The measured VSWR at 6.81 GHz is 1.21 dB, and the simulated radiation patterns, gain, and efficiency indicate excellent antenna performances.

Declaration of Competing Interest

The authors declare no conflicts of interest.

Acknowledgment

Financial supports from the National Natural Science Foundation of China under grant numbers (51802062, 51802280) and Postdoctoral Science Foundation of Zhejiang Province under grant number (ZJ2020008) are greatly appreciated.

Appendix A. Supplementary data

Supplementary material related to this article can be found, in the online version, at doi:https://doi.org/10.1016/j.jeurceramsoc.2021.03.052.

References

[1] M. Anab, M.I. Khattak, S.M. Owais, A.A. Khattak, A. Sultan, Design and analysis of millimeter wave dielectric resonator antenna for 5G wireless communication systems, Prog. Electromagn. Res. 98 (2020) 239–255.
[2] D. Wang, S. Zhang, G. Wang, Y. Vardaxoglou, W. Whittow, D. Cadman, D. Zhou, K. Song, I.M. Reaney, Cold sintered $CaTiO_3$-K_2MoO_4 microwave dielectric ceramics for integrated microstrip patch antennas, Appl. Mater. Today 18 (2020), 100519.
[3] H. Xiang, J. Kilpijärvi, S. Myllymäki, H. Yang, L. Fang, H. Jantunen, Spinel-olivine microwave dielectric ceramics with low sintering temperature and high quality factor for 5 GHz wi-fi antennas, Appl. Mater. Today 21 (2020), 100826.
[4] M.D. Hill, D.B. Cruickshank, Ceramic materials for 5G wireless communication systems, Am. Ceram. Soc. Bull. 98 (2019) 20–25.
[5] H. Ohsato, J. Varghese, A. Kan, J.S. Kim, I. Kagomiya, H. Ogawa, M.T. Sebastian, H. Jantunen, Volume crystallization and microwave dielectric properties of indialite/cordierite glass by TiO_2 addition, Ceram. Int. 47 (2021) 2735–2742.
[6] L. Li, C.H. Liu, J.Y. Zhu, X.M. Chen, B_2O_3-modified fused silica microwave dielectric materials with ultra-low dielectric constant, J. Eur. Ceram. Soc. 35 (2015) 1799–1805.
[7] M.T. Sebastian, H. Jantunen, Low loss dielectric materials for LTCC applications: a review, Int. Mater. Rev. 53 (2008) 57–90.
[8] D. Zhou, L.X. Pang, D.W. Wang, Z.M. Qi, I.M. Reaney, High quality factor, ultralow sintering temperature $Li6B_4O_9$ microwave dielectric ceramics with ultralow density for antenna substrates, ACS Sustain. Chem. Eng. 6 (2018) 11138–11143.
[9] W.B. Hong, L. Li, H. Yan, S.Y. Wu, H.S. Yang, X.M. Chen, Room-temperature-densified H_3BO_3 microwave dielectric ceramics with ultra-low permittivity and ultra-high Qf value, J. Materiomics 6 (2020) 233–239.
[10] K. Song, S. Wu, P. Liu, H. Lin, Z. Ying, P. Zheng, W. Su, J. Deng, L. Zheng, H. Qin, Phase composition and microwave dielectric properties of $SrTiO_3$ modified $Mg_2Al_4Si_5O_{18}$ cordierite ceramics, J. Alloys. Compd. 628 (2015) 57–62.
[11] M. Dong, Z. Yue, H. Zhuang, S. Meng, L. Li, Microstructure and microwave dielectric properties of TiO_2-doped Zn_2SiO_4 ceramics synthesized through the sol–gel process, J. Am. Ceram. Soc. 91 (2008) 3981–3985.
[12] K.X. Song, X.M. Chen, C.W. Zheng, Microwave dielectric characteristics of ceramics in Mg_2SiO_4–Zn_2SiO_4 system, Ceram. Int. 34 (2008) 917–920.
[13] M.E. Song, J.S. Kim, M.R. Joung, S. Nahm, Y.S. Kim, J.H. Paik, B.H. Choi, Synthesis and microwave dielectric properties of $MgSiO_3$ ceramics, J. Am. Ceram. Soc. 91 (2008) 2747–2750.
[14] S. Wu, Q. Ma, Synthesis, characterization and microwave dielectric properties of Zn_2GeO_4 ceramics, J. Alloys. Compd. 567 (2013) 40–46.
[15] C.X. Chen, S.P. Wu, Y.X. Fan, Synthesis and microwave dielectric properties of B_2O_3-doped Mg_2GeO_4 ceramics, J. Alloys. Compd. 578 (2013) 153–156.
[16] U. Došler, M.M. Kržmanc, D. Suvorov, The synthesis and microwave dielectric properties of $Mg_3B_2O_6$ and $Mg_2B_2O_5$ ceramics, J. Eur. Ceram. Soc. 30 (2010) 413–418.
[17] K.P. Surendran, P.V. Bijumon, P. Mohanan, M.T. Sebastian, (1-x)$MgAl_2O_4$-xTiO_2 dielectrics for microwave and millimeter wave applications, Appl. Phys. A 81 (2005) 823–826.
[18] K.P. Surendran, N. Santha, P. Mohanan, M.T. Sebastian, Temperature stable low loss ceramic dielectrics in (1-x)$ZnAlO_4$-xTiO_2 system for microwave substrate applications, Eur. Phys. J. B 41 (2004) 301–306.
[19] B. Liu, C.C. Hu, Y.H. Huang, H.B. Bafrooei, K.X. Song, Crystal structure, infrared reflectivity spectra and microwave dielectric properties of $CaAl_2O_4$ ceramics with low permittivity, J. Alloys. Compd. 791 (2019) 1033–1037.
[20] D. Thomas, M.T. Sebastian, Temperature-compensated $LiMgPO_4$: a new glass-free low-temperature cofired ceramic, J. Am. Ceram. Soc. 93 (2010) 3828–3831.
[21] J.J. Bian, D.W. Kim, K.S. Hong, Glass-free LTCC microwave dielectric ceramics, Mater. Res. Bull. 40 (2005) 2120–2129.
[22] X. Song, K. Du, J. Li, X. Lan, W. Lu, X. Wang, W. Lei, Low-fired fluoride microwave dielectric ceramics with low dielectric loss, Ceram. Int. 45 (2019) 279–286.
[23] X.Q. Song, W. Lei, Y.Y. Zhou, T. Chen, S.W. Ta, Z.X. Fu, W.Z. Lu, Ultra-low fired fluoride composite microwave dielectric ceramics and their application for $BaCuSi_2O_6$-based LTCC, J. Am. Ceram. Soc. 103 (2020) 1140–1148.
[24] Z. Zhang, Y. Tang, H. Xiang, A. Yang, Y. Wang, C. Yin, Y. Tian, L. Fang, $Li_5Ti_2O_6F$: a new low-loss oxyfluoride microwave dielectric ceramic for LTCC applications, J. Mater. Sci. 55 (2020) 107–115.
[25] R.G. Geyer, J.B. Jarvis, J. Krupka, Dielectric characterization of single-crystal LiF, CaF_2, MgF_2, BaF_2, and SrF_2 at microwave frequencies, Proceedings of Annual Report Conference on IEEE Electrical Insulation and Dielectric Phenomena, 2004, CEIDP'04 (2004) 493–497.
[26] H. Guo, A. Baker, J. Guo, C.A. Randall, Cold sintering process: a novel technique for low-temperature ceramic processing of ferroelectrics, J. Am. Ceram. Soc. 99 (2016) 3489–3507.
[27] L. Li, H. Yan, W.B. Hong, S.Y. Wu, X.M. Chen, Dense gypsum ceramics prepared by room-temperature cold sintering with greatly improved mechanical properties, J. Eur. Ceram. Soc. 40 (2020) 4689–4693.
[28] W.B. Hong, L. Li, M. Cao, X.M. Chen, Plastic deformation and effects of water in room-temperature cold sintering of NaCl microwave dielectric ceramics, J. Am. Ceram. Soc. 101 (2018) 4038–4043.
[29] D. Wang, B. Siame, S. Zhang, G. Wang, X. Ju, J. Li, Z. Lu, et al., Direct integration of cold sintered, temperature-stable $Bi_2Mo_2O_9$-K_2MoO_4 ceramics on printed circuit boards for satellite navigation antennas, J. Eur. Ceram. Soc. 40 (2020) 4029–4034.
[30] B. Liu, L. Li, K.X. Song, M.M. Mao, Z. Lu, G. Wang, L. Li, D. Wang, D. Zhou, A. Feteira, I.M. Reaney, Enhancement of densification and microwave dielectric properties in LiF ceramics via a cold sintering and post-annealing process, J. Eur. Ceram. Soc. 41 (2021) 1726–1729.
[31] E. Zhao, J. Hao, X. Xue, M. Si, J. Guo, H. Wang, Rutile TiO2 microwave dielectric ceramics prepared via cold sintering assisted two step sintering, J. Eur. Ceram. Soc. (2020), https://doi.org/10.1016/j.jeurceramsoc.2020.12.009.
[32] C.A. Schneider, W.S. Rasband, K.W. Eliceiri, NIH Image to ImageJ: 25 years of image analysis, Nat. Methods 9 (2012) 671–675.
[33] W.M. Haynes, CRC Handbook of Chemistry and Physics, CRS Press, 2017.
[34] L. Dressler, O. Wehrhan, X-ray double crystal diffractometer for testing of plane analyser crystals of LiF, Cryst. Res. Technol. 18 (1983) 1595–1598.
[35] M. Haug, F. Bouville, C.R. Agudo, J. Avaro, D. Gebauer, A.R. Studart, Cold densification and sintering of nanovaterite by pressing with water, J. Eur. Ceram. Soc. 40 (2020) 893–900.
[36] S.J. Penn, N.M. Alford, A. Templeton, X.R. Wang, M.S. Xu, M. Reece, K. Schrapel, Effects of porosity and grain size on the microwave dielectric properties of sintered alumina, J. Am. Ceram. Soc. 80 (1997) 1885–1888.
[37] S. Funahashi, J. Guo, H. Guo, K. Wang, A.L. Baker, K. Shiratsuyu, C.A. Randall, Demonstration of the cold sintering process study for the densification and grain growth of ZnO ceramics, J. Am. Ceram. Soc. 100 (2017) 546–553.
[38] I. Singh, V.S. Tripathi, Micro strip patch antenna and its applications: a survey, Int. J. Comp. Tech. Appl. 2 (2011) 1595–1599.
[39] S. Verma, L. Mahajan, R. Kumar, H.S. Saini, N. Kumar, A small microstrip patch antenna for future 5G applications, in: 2016 5th International Conference on Reliability, Infocom Technologies and Optimization (Trends and Future Directions) (ICRITO), IEEE, 2016, pp. 460–463.
[40] H.H. Guo, D. Zhou, C. Du, P.J. Wang, W.F. Liu, L.X. Pang, Q.P. Wang, J.Z. Su, C. Singh, S. Trukhanov, Temperature stable $Li_2Ti_{0.75}(Mg_{1/3}Nb_{2/3})_{0.25}O_3$-based microwave dielectric ceramics with low sintering temperature and ultra-low dielectric loss for dielectric resonator antenna applications, J. Mater. Chem. C Mater. Opt. Electron. Devices 8 (2020) 4690–4700.
[41] C. Du, H.H. Guo, D. Zhou, H.T. Chen, J. Zhang, W.F. Liu, J.Z. Su, H.W. Liu, Dielectric resonator antennas based on high quality factor $MgAl_2O_4$ transparent dielectric ceramics, J. Mater. Chem. C 8 (2020) 14880–14885.
[42] C. Yin, C. Li, G. Yang, L. Fang, Y. Yuan, L. Shu, J. Khaliq, $NaCa_4V_5O_{17}$: a low-firing microwave dielectric ceramic with low permittivity and chemical compatibility with silver for LTCC applications, J. Eur. Ceram. Soc. 40 (2020) 386–390.
[43] R. Umemura, H. Ogawa, H. Ohsato, A. Kan, A. Yokoi, Microwave dielectric properties of low-temperature sintered $Mg_3(VO_4)_2$ ceramic, J. Eur. Ceram. Soc. 25 (2005) 2865–2870.
[44] R. Naveenraj, E.K. Suresh, J. Dhanya, R. Ratheesh, Preparation and microwave dielectric properties of $Ba_3A(V_2O_7)_2$ (A = Mg, Zn) ceramics for ULTCC applications, Eur. J. Inorg. Chem. 2019 (2019) 949–955.